Predicting Grain Yield in Wheat Using UAV Multispectral and Ground Based Vegetation Indices

Vaibhav Malunjkar
Mahatma Phule Krishi Vidyapeeth
Sunil Kadam
Mahatma Phule Krishi Vidyapeeth
Pawan Kulwal
pawankulwal@gmail.com
Mahatma Phule Krishi Vidyapeeth

Research Article

Keywords: Wheat, UAV multispectral imaging, Vegetation indices, GreenSeeker, Grain yield prediction, Abiotic stress tolerance

Posted Date: March 24th, 2026

DOI: https://doi.org/10.21203/rs.3.rs-9015493/v1

Additional Declarations: No competing interests reported.

Abstract

High-throughput phenotyping using unmanned aerial vehicle (UAV) multispectral imagery offers a promising approach for predicting wheat yields under variable sowing conditions. This study evaluated the effectiveness of UAV-based vegetation indices compared to the GreenSeeker handheld sensor in estimating yield-related traits in 13 bread wheat genotypes. UAV-based multispectral indices—Normalized Difference Vegetation Index (NDVI), Green Normalized Difference Vegetation Index (GNDVI), Red-edge Normalized Difference Vegetation Index (RNDVI and simple ratio (SR) were captured using a MicaSense sensor at two growth stages [52 and 79 days after sowing (DAS) for timely sown; 16 and 43 DAS for late sown]. Simultaneously, NDVI was recorded using a GreenSeeker handheld sensor for direct comparison with UAV-derived NDVI. UAV-derived indices showed consistently stronger correlations with biological yield (BY), grain yield (GY), and thousand grain weight (TGW), particularly during the anthesis stage. GNDVI and SR emerged as the most predictive indices for BY and GY, while TGW showed stronger associations with early-stage indices. GreenSeeker NDVI correlations were weaker and less consistent across growth stages and sowing conditions. Genotypes such as Phule Samadhan, MACS 2496, and GS 4042 exhibited superior adaptability under late-sown heat stress, maintaining higher vegetation index values throughout. UAV-based multispectral imaging outperformed the handheld sensor in predicting key yield traits and detecting inter-genotypic variation under stress. Statistical and multivariate analyses (ANOVA, PCA, and heatmap visualization) revealed distinct inter-genotypic variability in vegetation indices, effectively distinguishing high-vigor and stress-susceptible wheat genotypes under varying sowing environments. These findings highlight UAV-based multispectral imaging as a robust, efficient, and scalable phenotyping tool for identifying stress-tolerant and high-yielding genotypes, underscoring the importance of phenological timing and optimal index selection in breeding and precision agriculture.

1 Introduction

Bread wheat (*Triticum aestivum* L.) is an important cereal crop for addressing global food security, serving as a staple for a significant portion of the world's population, including the majority of Indians. In India, wheat cultivation spans approximately over 31 million hectares, with an annual production exceeding 110 million tonnes, positioning the country as the second-largest wheat producer globally after China. However, recent years have witnessed a decline in wheat productivity, primarily attributed to abiotic stresses such as terminal heat stress, which adversely affect crop growth and yield in semi-arid regions substantially [16]. For instance, India's national average wheat yield declined from 3.48 t ha^{-1} in 2016–17 to 3.41 t ha^{-1} in 2021–22 due to rising temperatures during the grain-filling stage [13, 7].

Accurate yield prediction of wheat genotypes is vital for effective crop management and breeding programmes. Vegetation indices (VIs), which quantify plant health and vigor through spectral reflectance measurements, have become integral to crop phenotyping studies. Vegetation indices are estimated as the ratio of difference to sum of the sensor measurements in two bands. Indices such as the Normalized Difference Vegetation Index (NDVI) [29] and its variants, including the Green NDVI (GNDVI) and Red-edge NDVI (RNDVI), are extensively utilized to monitor crop status at various growth stages, offering insights into potential yield outcomes [39]. NDVI is widely used to assess vegetation health by comparing reflectance in the NIR and red bands. Its variant GNDVI [9] replaces the red band with the green band, making it more sensitive to chlorophyll concentration and nitrogen status. RNDVI [8] uses the red-edge band instead of the red band, enhancing sensitivity to canopy structure and photosynthetic activity.

Traditional methods of collecting data on vegetation indices using handheld sensors, such as spectroradiometers, are labour-intensive and often constrained by temporal and spatial limitations. In contrast, UAVs equipped with multispectral imaging systems have emerged as efficient tools for high-throughput phenotyping. UAV-based multispectral imagery enables rapid, non-invasive collection of high-resolution data across large fields, facilitating timely assessments of crop health and aiding in precision agriculture practices [42, 12, 1].

Several recent studies have explored the use of vegetation indices, particularly NDVI, for assessing crop health and predicting yield in wheat. Zsebő et al. [44] conducted a comparative evaluation of NDVI values obtained from GreenSeeker handheld sensors and UAV-mounted multispectral sensors, indicating that both platforms effectively predicted grain yield in winter wheat, especially when measurements were recorded around 226 days after sowing. Similarly, Walsh et al. [38] reported strong correlations (R^2 = 0.78) between NDVI values derived from UAV and handheld sensors at the Feekes 5 growth stage across multiple field trials in Idaho, indicating the viability of both systems for early-stage yield prediction. In a multi-temporal study, Camenzind and Yu [2] found that UAV-derived vegetation indices were highly effective in predicting wheat yield when collected near the flowering stage, emphasizing the importance of selecting optimal growth stages for spectral data acquisition.

Although several studies have shown the potential of UAVs for high-throughput phenotyping and yield estimation in wheat, most investigations have been limited to a single sowing environment or relied solely on UAV- or ground-based sensors in isolation. A systematic comparison of these sensing approaches under contrasting sowing conditions—timely and late—remains insufficiently documented. Such comparison is particularly important in regions where variations in sowing time expose the crop to distinct thermal regimes that markedly influence canopy development and grain formation. Further, the extent to which spectral responses differ among genotypes and across phenological stages such as booting and anthesis has not been clearly established. Addressing these gaps is critical for identifying reliable indices, improving the timing of image acquisition, and enhancing the biological interpretation of spectral signals across genotypes and environments. Therefore, the present study was undertaken to evaluate and compare UAV-based multispectral and handheld GreenSeeker measurements for predicting yield-related traits in wheat grown under timely and late sowing conditions, with specific attention to inter-genotypic variation and phenological sensitivity of vegetation indices.

2 Material and Methods

2.1 Plant Material

A set of 13 bread wheat (*Triticum aestivum* L.) genotypes comprising six advance breeding lines and seven released varieties developed at Mahatma Phule Krishi Vidyapeeth, Rahuri, Maharashtra, India were used in the present study. The released varieties were included as checks to represent widely cultivated material, while the advanced breeding lines were selected from ongoing breeding programs, based on their yield potential. The seeds were obtained from the Wheat Improvement Programme of MPKV Rahuri. The sowing of the experimental trial was done at the Climate Smart Research Block of the Centre for Advanced Agricultural Science and Technology for Climate Smart Agriculture and Water Management (CAAST-CSAWM), Mahatma Phule Krishi Vidyapeeth, Rahuri, Maharashtra, India (19°19'26.52" N latitude and 74°39'27.21" E longitude) during the wheat growing season of 2023-24 (Electronic Supplementary Material Fig. S1). The study area experiences a semi-arid climate with an annual average rainfall of 540 mm, predominantly occurring from June to September. The sowing was done at two different sowing dates. The sowing of the first trial (timely sown trial; TS) was done on November 24, 2023, while the second trial (late sown trial; LS) was done on December 30, 2023 so as to coincide the flowering of this trial with the elevated temperatures. Each genotype was sown in four rows of 1.5 m length with two replications. The row-to-row distance was kept as 20 cm and plant-to-plant 10 cm. The soil in the study area is classified as clay, comprising 20.92% sand, 23.08% silt, and 56% clay, with a bulk density of 1.27 g/cm^3. The experimental site is characterized by a nearly flat topography with uniform slope. Standard recommended agronomic practices were followed during the crop growth period. Irrigation was provided at critical stages to avoid water stress, and crop protection measures were undertaken as per standard recommendations.

2.2 UAV Image Acquisition

Aerial multispectral data were collected using a hexacopter drone/UAV equipped with a Altum-PT multispectral sensor (MicaSense Inc., USA). The multispectral sensor is equipped with Blue, Green, Red, Red-Edge, Near Infra-red, panchromatic and thermal sensors of 48^0 horizontal field of view (FOV) and 36.80 vertical FOV with a resolution of 3.2 megapixels. The multispectral sensor records the data in Blue, Green, Red, Red-Edge, Near Infra-red, and thermal bands independently covering the central wavelengths of 475 nm, 560 nm, 668 nm, 717 nm, 842 nm, and 10.5 μm, respectively. The sensor also records the panchromatic band with central wavelength of 634.5 nm [22].

The data acquisition flights were conducted at two different time points during key growth stages of the wheat crop. The first and second observations were recorded on 16 January 2024 and 12 February 2024 coinciding with 52nd day and 79th day after sowing of the timely sown trial, while 16th and 43rd day after sowing of the late sown trial. The two observation dates were deliberately selected to coincide with distinct and biologically significant phenological stages of wheat growth—approximately the booting or late-vegetative stage (around 52 DAS) and the anthesis stage (around 79 DAS) for the timely-sown trial, and the early-vegetative (around 16 DAS) and heading stages (around 43 DAS) for the late-sown trial—thereby capturing the spectral transitions associated with canopy expansion, photosynthetic activity, and the onset of reproductive development.

The UAV was operated at a consistent altitude of 25 meters above the crop canopy, with a flight speed of 3.5 m s^{-1} during data acquisition [42, 1]. Radiometric calibration was conducted by capturing an image of the calibrated reflectance panel before and after each flight using the multispectral sensor's integrated button [22]. To ensure accurate georeferencing of the UAV images, reference ground control points (GCPs) were recorded on-site using a handheld GPS device. All raw images were stored in .tiff format for subsequent processing.

2.3 Calculation of Vegetation Indices

The multispectral images collected through UAV were processed using Pix4D Mapper software (version 4.8.0) [24] to generate reflectance maps for various spectral bands, including Red, Green, Blue, NIR, and Red Edge. Vegetation indices such as NDVI, GNDVI, RNDVI, and SR were derived using the reflectance values from these bands. The formulae for the vegetation indices were used to quantify vegetation health and vigor by analyzing reflectance values from specific spectral bands captured through multispectral sensors. Standard formulae were added in the Pix4D Mapper index calculator [24] to generate NDVI, GNDVI, RNDVI, and SR. The formulae are presented in Table 1.

Table 1
Vegetation indices used in the study along with their formulae

Sr. No.	Vegetation Index	Formula	Reference
1.	Normalized Difference Vegetation Index (NDVI)	(NIR – Red) / (NIR + Red)	[29]
2.	Green Normalized Difference Vegetation Index (GNDVI)	(NIR – Green) / (NIR + Green)	[8]
3.	Red-edge Normalized Difference Vegetation Index (RNDVI)	(NIR – RedEdge) / (NIR + RedEdge)	[9]
4.	Simple Ratio (SR)	NIR / Red	[14]

The vegetation indices were selected for this study based on their strong biophysical association with canopy chlorophyll concentration, biomass accumulation, and photosynthetic activity in cereals. NDVI and GNDVI are widely used indicators of overall canopy greenness and nitrogen status, whereas RNDVI and SR provide greater sensitivity to early stress and structural variations in the canopy. Previous studies have demonstrated that these indices derived from UAV multispectral imagery are reliable predictors of wheat growth dynamics and grain yield under variable thermal and moisture regimes [30, 39, 44].

2.4 Ground Data Collection

Along with UAV-based NDVI, the study incorporated ground-based NDVI estimated using a handheld crop sensor, ‘GreenSeeker’ (Trimble, USA), following the manufacturer’s protocol [34] and established methods [28]. This instrument is used for on-field monitoring of crop health and vigour through direct measurement of NDVI under both timely and late sowing conditions. The GreenSeeker sensor measures the reflectance of light in the red and near-infrared (NIR) spectral regions and calculates NDVI. The GreenSeeker handheld crop sensor operates within specific spectral bands to calculate NDVI, focusing on the Red and NIR regions of the electromagnetic spectrum. The central wavelength for the GreenSeeker sensor is approximately 660 nm for the Red band and approximately 770 nm for the NIR band. The observations through GreenSeeker were taken on the same dates when the aerial observations were taken for the timely and late sowing conditions. UAV flights and GreenSeeker measurements were carried out between 10:00 a.m. and 12:00 p.m. local time under clear sky conditions to minimize variations in solar angle and illumination. The handheld sensor was held at a consistent height (30 cm) above the crop canopy to ensure uniform data collection and minimize variability. These measurements were further analysed for their correlation with biomass, grain yield, and other spectral indices to assess their utility in crop monitoring.

2.5 Observations on Yield and Yield Contributing Traits

Biological yield (BY) was measured as the total above-ground biomass, while grain yield (GY) was determined as the weight of threshed grains. 1000-grain weight (TGW) was measured by weighing 1,000 randomly selected grains from each genotype and replicate. These parameters were subsequently analyzed to assess the impact of sowing conditions on yield-related traits.

2.6 Analysis of Vegetation Indices

The data processing of the vegetation indices for the study was conducted using Pix4D mapper software (Version 4.8.0) [24], which involved multiple steps to ensure high-quality outputs. The 2443 and 2471 raw images recorded on January 16, 2024 (52 and 16 DAS) and February 12, 2024 (79 and 43 DAS), respectively were initially georeferenced using GPS data and stitched into a single image. Bundle block adjustment was performed, achieving a mean reprojection error of 0.165 pixels. A low-density point cloud was generated with 747,207 points and an average density of 533.01 points m^{-2}. Orthomosaic and Digital Surface Models (DSMs) were generated at a resolution of 1X GSD (0.992 cm $pixel^{-1}$) with surface smoothing and noise filtering was applied to enhance accuracy (Electronic Supplementary Material Fig. S2).

To ensure the reliability and consistency of spectral data, a comprehensive preprocessing and quality-control workflow was implemented prior to vegetation index calculation. Radiometric calibration was performed for each flight using calibrated reflectance panels captured before and after image acquisition to correct for illumination differences and atmospheric variability. All multispectral images were converted to surface reflectance units and normalized across bands using radiometric coefficients supplied by the sensor manufacturer. During orthomosaic generation, low-confidence pixels and boundary artifacts were automatically filtered using adaptive noise-suppression algorithms in Pix4D Mapper, followed by manual inspection to remove any residual shadows or specular reflections. Outliers arising from missing data, cloud shadows, or extreme reflectance values beyond three standard deviations from the mean were excluded to maintain data integrity. The final mosaics were then smoothed using a 3 × 3 mean filter to minimize local pixel noise while preserving spatial detail.

2.7 Inter-Genotypic Variability in Spectral Responses

To assess the extent of variability among genotypes, a one-way analysis of variance (ANOVA) was performed for each vegetation index (NDVI, GNDVI, RNDVI, and SR) under both sowing conditions using the *Genotype* factor as a fixed effect. Mean separation was carried out using Tukey's Honest Significant Difference (HSD) test at a 5% probability level to identify statistically distinct genotype groups. All statistical analyses were conducted using IBM SPSS Statistics (Version 26.0) and Microsoft Excel (2021). To visualize the multivariate relationships among genotypes and vegetation indices, the genotype-wise mean values of NDVI, GNDVI, RNDVI, and SR were standardized (z-scores) and subjected to principal component analysis (PCA) and hierarchical clustering. The PCA was performed using the *scikit-learn* library in Python (version 3.11), and the first two principal components (PC1 and PC2) were used to generate a biplot showing genotype clustering patterns under timely-sown (TS) and late-sown (LS) conditions. A heatmap of standardized vegetation indices was prepared using the *seaborn* visualization package to display relative differences among genotypes. Together, these analyses enabled statistical confirmation and visual interpretation of inter-genotypic variation in spectral responses and their association with canopy performance under different sowing conditions.

2.8 Correlation Analysis

The vegetation index values derived from UAV and GreenSeeker were statistically analyzed to evaluate their consistency and reliability in monitoring wheat growth and yield. The vegetation indices were correlated with biological yield, grain yield and TGW for both sowing conditions to identify significant relationships. Pearson correlation coefficients were calculated to quantify these associations, and comparative graphs were generated to visualize trends using MS Excel. Further, the ability of UAV-based indices and GreenSeeker NDVI to detect inter-genotype and intra-genotype variability was assessed.

3 Results

3.1 Yield Performance and Effect of Sowing Time

There was considerable variation for yield and yield-contributing traits among the wheat genotypes studied. Heat stress reduced wheat yield when sowing was delayed. The average biological yield was 8.97 t ha^{-1} under timely sowing and 9.58 t ha^{-1} under late sowing, while the average grain yield was 4.46 t ha^{-1} and 3.40 t ha^{-1} under timely and late sowing conditions, respectively. The thousand-grain weight (TGW) was 40.58 g and 29.38 g under timely and late sown conditions, respectively (Table 2).

Table 2
Details of wheat genotypes used along with their performance for yield and yield contributing traits

SN	Genotype	Source	Status	BY (t/ha)		GY (t/ha)		TGW (g)	
				TS	LS	TS	LS	TS	LS
1	GS 1003	BISA, Ludhiana	Breeding line	10.96	8.22	5.19	3.31	42.07	31.50
2	GS 2035	BISA, Ludhiana	Breeding line	9.57	10.25	4.74	3.73	41.19	32.57
3	GS 2051	BISA, Ludhiana	Breeding line	10.83	10.76	4.24	3.48	41.21	30.04
4	GS 9411	BISA, Ludhiana	Breeding line	10.50	8.36	5.36	2.69	39.45	26.09
5	GS 5444	BISA, Ludhiana	Breeding line	9.63	11.27	5.01	4.17	40.48	29.09
6	GS 4042	BISA, Ludhiana	Breeding line	10.32	10.92	4.43	4.38	40.29	31.41
7	Phule Samadhan	MPKV Rahuri	Released variety	8.05	10.70	3.46	3.56	39.55	30.42
8	HI 1605	IARI Regional Station, Indore	Released variety	6.61	10.93	3.17	4.06	41.10	27.77
9	HI 1633	IARI Regional Station, Indore	Released variety	10.20	7.48	5.05	2.26	43.65	29.69
10	MACS 2496	ARI, Pune	Released variety	8.05	8.78	3.90	3.15	42.08	29.50
11	MACS 6222	ARI, Pune	Released variety	5.47	10.19	3.55	4.23	38.08	30.73
12	NIAW 34	MPKV Rahuri	Released variety	7.87	8.38	4.83	2.65	39.05	26.71
13	Trimbak	MPKV Rahuri	Released variety	8.58	8.25	5.10	2.53	39.35	26.40
	Mean			8.97	9.58	4.46	3.40	40.58	29.38
	SD			1.70	1.34	0.73	0.71	1.51	2.08
	CV (%)			18.98	13.98	16.47	20.82	3.73	7.07

BY, biological yield; GY, grain yield; TGW, 1000 grain weight; TS, timely sown trial; LS, late sown trial; SD, standard deviation; CV, coefficient of variation

Although biological yield was slightly higher under late sowing, this was not reflected in grain yield due to a substantial reduction in TGW. The breeding lines performed comparatively better than the released varieties under both timely and late sowing conditions. Only three varieties (Phule Samadhan, HI 1605, and MACS 6222) yielded higher under late sowing than under timely sowing conditions.

3.2 Spatial Variability and Vegetation Health from UAV Imagery

There was distinct spatial variation in vegetation health across the wheat crop under timely and late sowing conditions. Under timely sowing (TS), vegetation appeared denser and more uniformly distributed, indicative of healthier and well-established crop growth. In contrast, late sowing (LS) showed lower vegetation density and reduced uniformity, suggesting delayed growth due to late planting. Over time, as observed between the two flight dates, vegetation density improved under both sowing conditions (Figs. 1 and 2).

Spatial distribution maps of NDVI, GNDVI, RNDVI, and SR derived from UAV-based multispectral imagery at 52 DAS under TS and 16 DAS under LS are presented in Fig. 1. NDVI and GNDVI maps indicated vegetation greenness and chlorophyll status, respectively, with higher values (> 0.80) prominently observed in TS plots. RNDVI illustrated chlorophyll variations and canopy structural differences, while SR values, representing biomass accumulation, were notably higher in TS plots (> 10).

Figure 2 shows the spatial distribution of indices at 79 DAS under TS and 43 DAS under LS conditions. NDVI and GNDVI maps indicated robust growth in TS plots, with values predominantly > 0.80, whereas LS plots showed comparatively lower vigour. RNDVI highlighted genotypic differences in chlorophyll content and canopy structure, and SR reflected higher biomass accumulation in TS compared to LS plots.

3.3 Temporal Trends of Vegetation Indices

Under TS, vegetation indices (Table 3) showed strong canopy health, with NDVI ranging from 0.84–0.91 in the first observation and 0.66–0.79 in the second. GNDVI, RNDVI, and SR also declined over time. Genotypes GS 4042, Phule Samadhan, and MACS 2496 consistently showed higher index values. Under LS (Table 4), early stress resulted in low NDVI values (0.34–0.57), but most genotypes recovered by the second observation (0.79–0.90). SR values peaked for MACS 2496 (23.22). Phule Samadhan, GS 4042, and MACS 2496 showed resilience across sowing conditions.

Table 3
Vegetation indices estimated using multispectral sensor for 13 wheat genotypes in the timely sown condition

Genotype	Vegetation indices							
	First Observation (52 DAS)				Second Observation (79 DAS)			
NDVI	GNDVI	RNDVI	SR	NDVI	GNDVI	RNDVI	SR	
GS 1003	0.90	0.77	0.52	20.69	0.77	0.68	0.41	8.31
GS 2035	0.89	0.77	0.52	20.84	0.74	0.66	0.39	7.61
GS 2051	0.88	0.75	0.50	18.52	0.73	0.65	0.39	7.42
GS 9411	0.89	0.75	0.48	19.99	0.77	0.68	0.41	8.53
GS 5444	0.90	0.76	0.50	19.57	0.73	0.64	0.37	7.09
GS 4042	0.91	0.77	0.51	23.07	0.79	0.69	0.43	9.04
Phule Samadhan	0.91	0.78	0.52	23.08	0.74	0.65	0.40	7.51
HI 1605	0.88	0.76	0.51	17.52	0.66	0.58	0.34	5.28
HI 1633	0.90	0.79	0.56	19.52	0.73	0.65	0.44	6.89
MACS 2496	0.91	0.79	0.55	23.30	0.71	0.63	0.43	6.70
MACS 6222	0.85	0.72	0.46	14.55	0.71	0.61	0.42	6.20
NIAW 34	0.84	0.71	0.45	13.80	0.68	0.60	0.42	5.63
Trimbak	0.88	0.76	0.53	18.55	0.75	0.67	0.50	7.50
Mean	0.89	0.76	0.51	19.46	0.73	0.65	0.41	7.21
SD	0.02	0.02	0.03	2.98	0.04	0.03	0.04	1.09
CV (5%)	2.48	3.13	6.21	15.29	4.92	5.12	9.24	15.14

Table 4
Vegetation indices estimated using multispectral sensor for 13 wheat genotypes under late sown condition

Genotype	Vegetation indices							
	First Observation (16 DAS)				Second Observation (43 DAS)			
NDVI	GNDVI	RNDVI	SR	NDVI	GNDVI	RNDVI	SR	
GS 1003	0.43	0.45	0.22	3.06	0.79	0.65	0.39	10.62
GS 2035	0.57	0.53	0.27	4.53	0.89	0.74	0.49	18.16
GS 2051	0.50	0.49	0.25	3.43	0.87	0.73	0.48	16.27
GS 9411	0.46	0.47	0.23	3.06	0.86	0.72	0.47	16.23
GS 5444	0.43	0.46	0.22	2.84	0.87	0.76	0.52	17.23
GS 4042	0.53	0.51	0.26	4.08	0.89	0.78	0.55	20.92
Phule Samadhan	0.46	0.47	0.23	3.06	0.90	0.78	0.54	21.61
HI 1605	0.36	0.42	0.19	2.23	0.89	0.76	0.51	19.61
HI 1633	0.34	0.42	0.19	2.18	0.85	0.73	0.46	14.76
MACS 2496	0.54	0.51	0.26	4.29	0.90	0.78	0.53	23.22
MACS 6222	0.38	0.43	0.20	2.37	0.89	0.77	0.51	20.03
NIAW 34	0.39	0.43	0.20	2.43	0.87	0.75	0.48	17.04
Trimbak	0.34	0.41	0.18	2.13	0.88	0.76	0.49	18.28
Mean	0.44	0.46	0.22	3.05	0.87	0.75	0.49	18.00
SD	0.08	0.04	0.03	0.82	0.03	0.04	0.04	3.27
CV (%)	17.59	8.52	13.50	26.91	3.35	4.75	8.41	18.16

3.4 Inter-genotypic variation in vegetation indices

Analysis of variance (ANOVA) revealed significant ($P < 0.05$) differences among genotypes for all vegetation indices under both sowing conditions, confirming substantial inter-genotypic variability in spectral response. The heatmaps of standardized indices (Fig. 3a,b) clearly distinguished high-performing genotypes—Phule Samadhan, MACS 2496, and GS 4042—which maintained higher NDVI, GNDVI, and SR values across growth stages, from low-performing genotypes such as Trimbak and NIAW 34, which recorded lower reflectance under late-sown conditions.

Principal Component Analysis (PCA) of standardized vegetation indices (Fig. 4) explained 92.2% of the total variance by PC1 and 6.2% by PC2, effectively summarizing multidimensional spectral variability among genotypes. The PCA biplot revealed a clear separation between TS and LS conditions, with genotypes clustering according to sowing environment. High-vigor genotypes (Phule Samadhan, GS 4042, MACS 2496) clustered toward the positive PC1 axis, while low-vigor and stress-susceptible lines (NIAW 34, HI 1605, Trimbak) occupied the opposite quadrant. This separation indicates that UAV-derived vegetation indices effectively capture environmental effects and genotypic responses, consistent with the patterns observed in the heatmaps.

3.5 Comparison Between UAV- and Ground-Based NDVI

GreenSeeker NDVI (Table 5) was consistently higher under TS than LS. Genotypes GS 4042, GS 2051, and Phule Samadhan maintained high NDVI across both sowing conditions, while Trimbak and NIAW 34 showed sensitivity under LS.

Table 5
NDVI measured using GreenSeeker crop sensor for 13 wheat genotypes under timely and late sown conditions

Genotype	NDVI			
	Timely Sowing		Late Sowing	
First Observation (52 DAS)	**Second Observation (79 DAS)**	**First Observation (16 DAS)**	**Second Observation (43 DAS)**	
GS 1003	0.81	0.82	0.61	0.82
GS 2035	0.81	0.79	0.57	0.79
GS 2051	0.82	0.82	0.59	0.82
GS 9411	0.83	0.81	0.57	0.81
GS 5444	0.81	0.80	0.61	0.80
GS 4042	0.84	0.83	0.53	0.83
Phule Samadhan	0.83	0.82	0.56	0.82
HI 1605	0.78	0.79	0.62	0.79
HI 1633	0.76	0.81	0.58	0.81
MACS 2496	0.82	0.79	0.60	0.79
MACS 6222	0.82	0.77	0.61	0.77
NIAW 34	0.78	0.78	0.58	0.78
Trimbak	0.81	0.76	0.61	0.76
Mean	0.81	0.80	0.59	0.80
SD	0.02	0.02	0.03	0.02
CV (%)	2.83	2.68	4.40	2.68

Comparison of UAV and GreenSeeker NDVI showed similar trends (Fig. 5a,b), although UAV values were generally higher under TS and more variable under LS. Both sensors identified similar genotype performance patterns; however, UAV NDVI appeared more sensitive to spatial variability due to its higher spatial resolution. This can be attributed to differences in the scale and geometry of measurements. The UAV captured reflectance data over the entire plot from above, integrating canopy-level variability, while the GreenSeeker recorded point-based readings along crop rows at a fixed height. Variations in canopy structure, row spacing, and soil background influence the ground sensor more strongly, whereas UAV-based imaging averages reflectance across a larger area. Similar discrepancies between UAV and proximal sensors have been reported in earlier studies [12, 40].

3.6 Correlation of Vegetation Indices with Yield Attributes

In both trials, grain yield showed significant positive correlations with biological yield and TGW. The correlations were stronger under late-sown conditions than under timely-sown conditions (Table 6). Vegetation indices derived from UAV imagery showed significant correlations with yield attributes, whereas handheld NDVI exhibited comparatively weaker relationships. Early-stage indices were better predictors of TGW, while later-stage indices were more predictive of biological yield and grain yield.

Table 6
Correlations between different vegetation indices and yield and TGW

Trait/ Vegetation index	BY	GY	TGW	NDVI Handheld	NDVI	GNDVI	RNDVI
TS trial (first observation)							
GY	0.709**						
TGW	0.497	0.173					
NDVI (Handheld)	0.148	-0.107	-0.430				
NDVI	0.465	0.041	0.529	0.360			
GNDVI	0.449	0.042	0.777*	0.032	0.913**		
RNDVI	0.290	0.057	0.758*	-0.157	0.763**	0.929**	
SR	0.475	0.019	0.438	0.485	0.962**	0.868**	0.692*
LS trial (first observation)							
GY	0.892**						
TGW	0.375	0.537					
NDVI (Handheld)	0.204	0.157	0.358				
NDVI	0.347	0.337	0.535	0.360			
GNDVI	0.367	0.362	0.557*	0.387	0.996**		
RNDVI	0.361	0.364	0.566*	0.363	0.996**	0.998**	
SR	0.283	0.319	0.576*	0.315	0.985**	0.978**	0.983**
TS trial (second observation)							
NDVI (Handheld)	-0.331	-0.067	0.089				
NDVI	0.728**	0.529	0.062	-0.488			
GNDVI	0.808**	0.598*	0.177	-0.471	0.979**		
RNDVI	0.067	0.409	-0.154	-0.098	0.332	0.356	
SR	0.751**	0.493	0.077	-0.536	0.992**	0.972**	0.270
LS trial (second observation)							
NDVI (Handheld)	0.204	0.157	0.358				
NDVI	0.505	0.301	-0.056	-0.267			
GNDVI	0.513	0.362	-0.081	-0.257	0.968**		

Trait/ Vegetation index	BY	GY	TGW	NDVI Handheld	NDVI	GNDVI	RNDVI
RNDVI	0.623*	0.495	0.011	-0.108	0.926**	0.977**	
SR	0.451	0.372	0.012	-0.216	0.930**	0.937**	0.925**

BY, biological yield; GY, grain yield; TGW, 1000 grain weight; TS, timely sown trial; LS, late sown trial

*, ** significant at $P < 0.05$ and 0.01, respectively

4 Discussion

The study demonstrates the differential impact of heat stress on wheat genotypes and the advantage of timely sowing. Despite higher biological yield under late sowing, TGW and grain yield were compromised. This finding aligns with previous reports where delayed planting exposed the crop to terminal heat stress, particularly during grain filling, thereby reducing grain yield and TGW [26, 6, 33, 16].

The vegetation indices derived from UAV imaging highlighted spatial variability and enabled genotype differentiation. UAV-based NDVI demonstrated greater sensitivity and spatial resolution compared to handheld GreenSeeker. The UAV sensor captures canopy-level reflectance across entire plots with a nadir viewing angle and high spatial resolution, effectively averaging heterogeneity and reducing soil background influence. In contrast, the GreenSeeker records point-based readings along crop rows at a fixed height, making it more sensitive to row spacing, plant gaps, and soil reflectance. Additionally, sensor calibration methods, instantaneous illumination, and atmospheric scattering can cause slight radiometric mismatches between systems. Environmental conditions—such as sun angle, wind-induced canopy movement, or transient shading—also contribute to temporal variability. Similar discrepancies between UAV- and ground-based NDVI have been reported earlier [12, 40, 3]. Zsebő et al. [44] also reported significant differences between NDVI values obtained from GreenSeeker and those derived from UAV-mounted multispectral cameras, emphasizing the importance of sensor type and measurement methodology in NDVI assessments. Veverka et al. [36] highlighted the strength of red-edge NDVI in capturing subtle canopy differences that traditional NDVI may overlook. Their findings support the observations in this study, where RNDVI maps distinguished inter-genotypic variation in chlorophyll content and structural traits, especially under stress conditions. Given its sensitivity to leaf biochemistry and architecture, RNDVI is particularly useful for identifying genotypes with higher resilience to heat or nutrient stress. Its sensitivity to variations in the red-edge region (700–740 nm) enables better detection of moderate chlorophyll depletion and early senescence compared to red-based NDVI. Similar findings were reported by Zarco-Tejada et al. [41], Costa et al. [4], and Veverka et al. [36], who highlighted red-edge indices as robust indicators of physiological stress and genotype discrimination in cereals.

The clustering of genotypes based on vegetation indices shows the potential of UAV-based spectral phenotyping for discriminating genotypes under varying conditions. Similar spectral differentiation among wheat genotypes under heat stress has been reported by Costa et al. [4], Sharma et al. [30], and Veloo et al. [35]. The consistent grouping of Phule Samadhan, MACS 2496, and GS 4042 across sowing conditions suggests robust canopy maintenance and higher resilience to terminal stress, corroborating their superior yield performance. Strong correlations between UAV-derived vegetation indices (particularly GNDVI and SR) and yield parameters such as biological yield and grain yield, especially during the anthesis stage, confirm the importance of temporal precision in phenotyping. The anthesis period is critical for assimilate partitioning and grain development, making it a key time window for spectral data acquisition. Sun et al. [32] demonstrated that UAV-based hyperspectral indices captured during anthesis were significantly correlated with final wheat yield, a finding supported by Liu et al. [19], who observed that multi-temporal vegetation indices acquired at heading and flowering stages offered the highest predictive power in wheat yield modelling.

Among all indices, NDVI emerged as a robust standalone parameter, demonstrating consistently strong correlations with other vegetation indices (GNDVI, RNDVI, SR) as well as with yield-related traits. This supports the conclusions of Kyratzis et al. [17], who identified NDVI as a versatile index for UAV-based wheat phenotyping capable of detecting both spatial and temporal crop variability. Similarly, Moghimi et al. [23] emphasized that NDVI, due to its simplicity, spectral sensitivity, and wide dynamic range, continues to be a central indicator for high-throughput phenotyping systems.

Importantly, Walsh et al. [38] confirmed that while both UAV-mounted and handheld sensors like GreenSeeker effectively estimated wheat yield, UAV-derived NDVI exhibited superior spatial resolution, consistency, and repeatability across varying environments. Additionally, Rehman et al. [25] reported that UAV-derived NDVI offered more consistent and temporally stable data for monitoring spatial variability in crop health and predicting yield. The present study noted that the correlations were more pronounced during the second observation period, aligning with the anthesis stage of wheat growth, which is critical for yield determination. However, NDVI values recorded using handheld sensors had weaker correlations with yield components, suggesting limitations in their predictive capabilities compared to multispectral sensors. Additionally, TGW was better predicted by UAV indices captured during earlier growth stages (vegetative to booting). This pattern is consistent with findings of Zhu et al. [43], who reported that early-stage vegetation indices (including NDVI and SR) showed stronger associations with grain size and weight, likely due to their reflection of canopy vigor and early assimilate capacity. Furthermore, the higher biological yield but lower grain yield observed in late-sown wheat can be attributed to altered assimilate partitioning under terminal heat stress. Late-sown wheat accumulates greater vegetative biomass during early stages, but elevated temperatures during reproductive growth reduce translocation of assimilates to grains, resulting in a higher straw-to-grain ratio. Similar differences in partitioning efficiency between vegetative and reproductive sinks under late sowing have been reported previously [20, 27].

In addition to yield prediction, UAV-based vegetation indices have the potential to map spatial variability in nutrients and moisture, thereby enabling site-specific management interventions. Although this was not within the scope of the present study, it provides a useful direction for future research.

As the present study demonstrates the applicability of UAV-based multispectral indices for assessing wheat canopy dynamics and predicting yield performance, a few limitations should be acknowledged. The analysis was confined to a single growing season and two sowing conditions, which may not fully capture inter-annual climatic variability. Yield estimation was based on linear correlations, and future work should integrate machine-learning or hybrid regression approaches such as PLSR, Random Forest, or deep neural models to enhance predictive accuracy. Scaling up this framework to larger spatial extents or operational farmer fields will require automation of image calibration, georeferencing using RTK-enabled UAVs, and standardized data processing pipelines. Long-term multi-environment testing, incorporation of hyperspectral or thermal sensors, and integration with ground-based physiological and genomic data will further strengthen the utility of UAV-assisted phenotyping for precision breeding and stress-resilient crop management.

5 Conclusions

The study concludes that vegetation indices recorded using multispectral sensors demonstrated stronger predictive relationships with yield and yield-contributing traits compared to handheld sensors during the later stages of crop growth across 13 wheat genotypes, including both released varieties and advanced breeding lines. However, these indices showed greater efficiency in predicting thousand-grain weight (TGW) at earlier growth stages than at later stages. This suggests that vegetation indices recorded during the anthesis stage provide better estimates of grain yield, whereas indices captured at the peak vegetative stage provide better estimates of TGW.

The integration of UAV-based multispectral imaging with ground-based sensing provides a rapid and scalable approach for wheat phenotyping. This approach is particularly valuable for breeding programs, as it enables non-destructive, high-throughput screening of large numbers of genotypes across different environments. Statistical and multivariate analyses clearly revealed inter-genotypic differences in spectral response, with high-performing genotypes such as Phule Samadhan, MACS 2496, and GS 4042 exhibiting consistently higher vegetation indices and clustering distinctly from stress-susceptible lines. These findings support the robustness of UAV-derived indices, particularly RNDVI and SR, in capturing physiological resilience and canopy vigor across phenological stages.

The combined use of ANOVA, PCA, and heatmap visualization strengthened the interpretation of spectral variability and highlighted the potential of UAV-based phenotyping for rapid screening and selection of stress-tolerant wheat genotypes in breeding and precision agriculture programs. In the short term, UAV-based multispectral imaging and ground-based GreenSeeker measurements can assist farmers and extension agencies in timely crop performance assessments and yield prediction. In the long term, integrating UAV-derived vegetation indices into breeding pipelines can accelerate the selection of high-yielding and stress-resilient genotypes through non-destructive, high-throughput phenotyping.

Furthermore, coupling UAV observations with soil and weather data may enable site-specific nutrient and irrigation management, contributing to the broader adoption of precision agriculture practices.

Declarations

Funding

Funding was provided by the Department of Biotechnology (DBT), Government of India (Grant No. 102/1FD/SAN/3963/2019-20 dated 29.02.2020); the Indian Council of Agricultural Research (ICAR), New Delhi (Grant No. NAHEP/CAAST/2018-19/04 dated 13.06.2018); and the Government of Maharashtra (Grant No. MPV1422/L.No.253/7-A dated 21.03.2023).

Ethics Approval and Consent to Participate

The wheat genotypes used in this study were cultivated as part of a field experiment at Mahatma Phule Krishi Vidyapeeth Rahuri, Maharashtra (India). The plant materials were obtained from the wheat breeding program of MPKV Rahuri and were grown under standard agronomic practices. The collection and use of plant materials complied with all relevant institutional national and international guidelines.

Permission Statement

The plant materials used in this study were obtained from the wheat breeding programme of Mahatma Phule Krishi Vidyapeeth Rahuri. No special permits were required for the use of these cultivated plant materials in experimental research.

Consent for Publication

Not applicable.

Competing Interests

The authors declare no competing interests.

Author Contribution

PK: Conceptualization, Funding acquisition, Resources, Supervision, Visualization, Study design, Data curation, Formal analysis, Investigation, Methodology, Writing – original draft. SK: Conceptualization, Funding acquisition, Resources, Software, Study design, Writing – review & editing. VM: Data curation, Data analysis, Methodology, Writing – review & editing.

Acknowledgement

The authors acknowledge the assistance provided by the field staff associated with the DBT-funded wheat research project.

Data Availability

The datasets generated and analyzed during the current study are available from the corresponding author on reasonable request.

References

1. Adao T, Hruška J, Pádua L, Bessa J, Peres E, Morais R, et al. Hyperspectral imaging: A review on UAV-based sensors, data processing and applications for agriculture and forestry. Remote Sens. 2017;9(11):1110.
2. Camenzind MP, Yu K. Multi-temporal multispectral UAV remote sensing allows for yield assessment across European wheat varieties already before flowering. Front Plant Sci. 2024;14:1214931. 10.3389/fpls.2023.1214931.
3. Condorelli GE, Marco M, Maria N, Pedro AS, White JW, French AN, et al. Comparative aerial and ground-based high throughput phenotyping for the genetic dissection of NDVI as a proxy for drought adaptive traits in durum wheat. Front Plant Sci. 2018;9:893. 10.3389/fpls.2018.00893.
4. Costa C, Araus JL, Kefauver SC. UAV-based hyperspectral imaging and functional regression for assessing wheat genotypes under heat stress environments. Precis Agric. 2022;23(5):1176–93. 10.1007/s11119-021-09852-5.
5. Duan T, Zheng B, Guo W, Ninomiya S, Guo Y. Comparison of handheld and UAV-based hyperspectral remote sensing for estimating yield-related traits in wheat. Field Crops Res. 2017;210:213–25.
6. Farooq M, Bramley H, Palta JA, Siddique KHM. Heat stress in wheat during reproductive and grain-filling phases. Crit Rev Plant Sci. 2011;30:491–507. 10.1080/07352689.2011.615687.
7. FAOSTAT. FAOSTAT statistical database. Rome: Food and Agriculture Organization of the United Nations; 2023.
8. Gitelson AA, Kaufman YJ, Merzlyak MN. Use of a green channel in remote sensing of global vegetation from EOS-MODIS. Remote Sens Environ. 1996;58:289–98. 10.1016/S0034-4257(96)00072-7.
9. Gitelson AA, Merzlyak MN. Remote estimation of chlorophyll content in higher plant leaves. Int J Remote Sens. 1997;18:2691–7. 10.1080/014311697217558.
10. Hassan MA, Yang M, Rasheed A, Jin X, Xia X, Xiao Y, et al. Time-series multispectral indices from unmanned aerial vehicle imagery reveal senescence rate in bread wheat. Remote Sens. 2018;10:809. 10.3390/rs10060809.

11. Heinemann P, Prey L, Hanemann A, Ramgraber L, Seidl-Schulz J, Noack PO. Enhancing model performance through data fusion in multispectral and RGB image-based field phenotyping of wheat grain yield. Precis Agric. 2025;26:20. 10.1007/s11119-024-10211-3.
12. Hunt ER, Hively WD, Fujikawa SJ, Linden DS, Daughtry CS, McCarty GW. Acquisition of NIR-green-blue digital photographs from unmanned aircraft for crop monitoring. Remote Sens. 2010;2(1):290–305.
13. ICAR. Annual wheat report 2022-23. New Delhi: Indian Council of Agricultural Research; 2023.
14. Jordan CF. Derivation of leaf area index from quality of light on the forest floor. Ecology. 1969;50:663–6. 10.2307/1936256.
15. Khan Z, Eichi VR, Haefele S, Garnett T, Miklavcic SJ. Estimation of vegetation indices for high-throughput phenotyping of wheat using aerial imaging. Plant Methods. 2018;14:20. 10.1186/s13007-018-0287-6.
16. Kumar S, Jacob SR, Mir RR, Vikas VK, Kulwal P, Chandra T, et al. Indian wheat genomics initiative for harnessing the potential of wheat germplasm resources for breeding disease-resistant, nutrient-dense, and climate-resilient cultivars. Front Genet. 2022;13:834366. 10.3389/fgene.2022.834366.
17. Kyratzis A, Pateras D, Sidiropoulos E, Moshou D. UAV-based multispectral imaging for wheat phenotyping. Remote Sens. 2023;16:3710. 10.3390/rs16193710.
18. Li F, Mistele B, Schmidhalter U. Application of GreenSeeker for yield prediction in wheat. Sensors. 2019;19:1108. 10.3390/s19051108.
19. Liu Y, Sun L, Liu B, Wu Y, Ma J, Zhang W, et al. Estimation of winter wheat yield using multiple temporal vegetation indices derived from UAV-based multispectral and hyperspectral imagery. Remote Sens. 2023;15:4800. 10.3390/rs15194800.
20. Lobell DB, Gourdji SM. The influence of climate change on global crop productivity. Plant Physiol. 2012;160:1686–97.
21. Martin KL, Kitchen NR, Sudduth KA, Drummond ST, Wiebold WJ. Canopy reflectance-based nitrogen sensing for winter wheat. Agron J. 2012;104:159–66. 10.2134/agronj2011.0244.
22. MicaSense. Altum-PT integration guide. Seattle: MicaSense Inc.; 2022.
23. Moghimi A, Bhatnagar A, Bhadra S, Dodla S, Ray JD. High-throughput yield phenotyping in wheat using UAV-based hyperspectral imaging. Remote Sens. 2019;11:483. 10.3390/rs11050483.
24. Pix4D. Pix4Dmapper software manual. Lausanne: Pix4D SA; 2023.
25. Rehman T, Shi Y, Hussain HA, Liu J. Sensitivity of vegetation indices derived from unmanned aerial vehicles and handheld sensors in predicting wheat traits. Remote Sens. 2022;14:512. 10.3390/rs14122770.
26. Reynolds MP, Bonnett D, Chapman SC, Furbank RT, Manès Y, Mather DE, et al. Raising yield potential of wheat. II. Increasing photosynthetic capacity and efficiency. J Exp Bot. 2010;61:3211–22.
27. Reynolds MP, Langridge P. Physiological breeding. Curr Opin Plant Biol. 2016;31:162–71.

28. Raun WR, Solie JB, Johnson GV, Stone ML, Mullen RW, Freeman KW, et al. Improving nitrogen use efficiency in cereal grain production with optical sensing and variable rate application. Agron J. 2002;94:815–20.
29. Rouse JW, Haas RH, Schell JA, Deering DW. Monitoring vegetation systems in the Great Plains with ERTS. In: Third Earth Resources Technology Satellite-1 Symposium; 1974. pp. 309–317.
30. Sharma R, Singh G, Bhatia VS, Saini HS, Sandhu SS. Phenotyping wheat genotypes for heat stress tolerance using physiological traits and UAV-based multispectral imagery. Comput Electron Agric. 2024;220:108637.
31. Singh A, Ganapathysubramanian B, Singh AK, Sarkar S. Integrating UAV-based imaging with machine learning to predict wheat yield. Agric Syst. 2021;187:103027. 10.1016/j.agsy.2020.103027.
32. Sun Y, Wang H, Zhang C, Shang J, Liu J. High-throughput phenotyping of wheat yield using UAV-based hyperspectral imagery. Remote Sens Environ. 2020;237:111872. 10.1016/j.rse.2019.111872.
33. Tiwari T, Singh D, Lal GM. Effect of dates of sowing and varieties on growth and yield of wheat (Triticum aestivum L). Int J Agric Sci. 2012;8:91–4.
34. Trimble. GreenSeeker handheld crop sensor user guide. Sunnyvale: Trimble Inc.; 2022.
35. Veloo R, Shepley T, Reynolds MP. UAV-derived digital trait analysis for consistent representation of wheat grain yield and adaptability across variable environments. Appl Eng Agric. 2024;40(3):415–26.
36. Veverka D, Smid M, Brovkina O, Kovács T, Urban O. Evaluating red-edge indices for quantifying canopy stress and chlorophyll variability in wheat. Field Crops Res. 2023;298:109002.
37. Veverka M, Pospíšilová J, Zemek F. UAV-based red-edge NDVI as a proxy for assessing grain protein content in spring wheat. Agronomy. 2023;13:207. 10.3390/agronomy13010207.
38. Walsh OS, Knighton JE, Johnson GV. Use of NDVI sensors (UAV and GreenSeeker) to predict wheat yield across multiple environments. University of Idaho Extension Bulletin BUL 1033; 2022. Available from: https://www.uidaho.edu/-/media/UIdaho-Responsive/Files/Extension/publications/bul/bul1033.PDF. Accessed 24 May 2025.
39. Wu R, Fan Y, Zhang L, Yuan D, Gao G. Wheat yield estimation study using hyperspectral vegetation indices. Appl Sci. 2024;14:4245. 10.3390/app14104245.
40. Yu N, Li L, Schmitz N, Tian LF, Greenberg JA, Diers BW. Development of methods to improve soybean yield estimation and predict plant maturity with UAV-based imagery. Remote Sens Environ. 2016;187:91–101.
41. Zarco-Tejada PJ, Miller JR, Morales A, Berjón A, Agüera J. Hyperspectral indices and model inversion for chlorophyll content estimation in vegetation. Remote Sens Environ. 2003;84:562–75.
42. Zhang C, Kovacs JM. The application of small unmanned aerial systems for precision agriculture: A review. Precis Agric. 2012;13(6):693–712.
43. Zhu Q, Sun J, Wang X, Wang Y. Prediction of wheat yield using vegetation indices derived from UAV multispectral imagery under varying sowing conditions. Agronomy. 2024;14:991.

10.3390/agronomy14050991.

44. Zsebő S, Bede L, Kukorelli G, Kulmány IM, Milics G, Stencinger D, et al. Yield prediction using NDVI values from GreenSeeker and MicaSense cameras at different stages of winter wheat phenology. Drones. 2024;8:88. 10.3390/drones8030088.

Figures

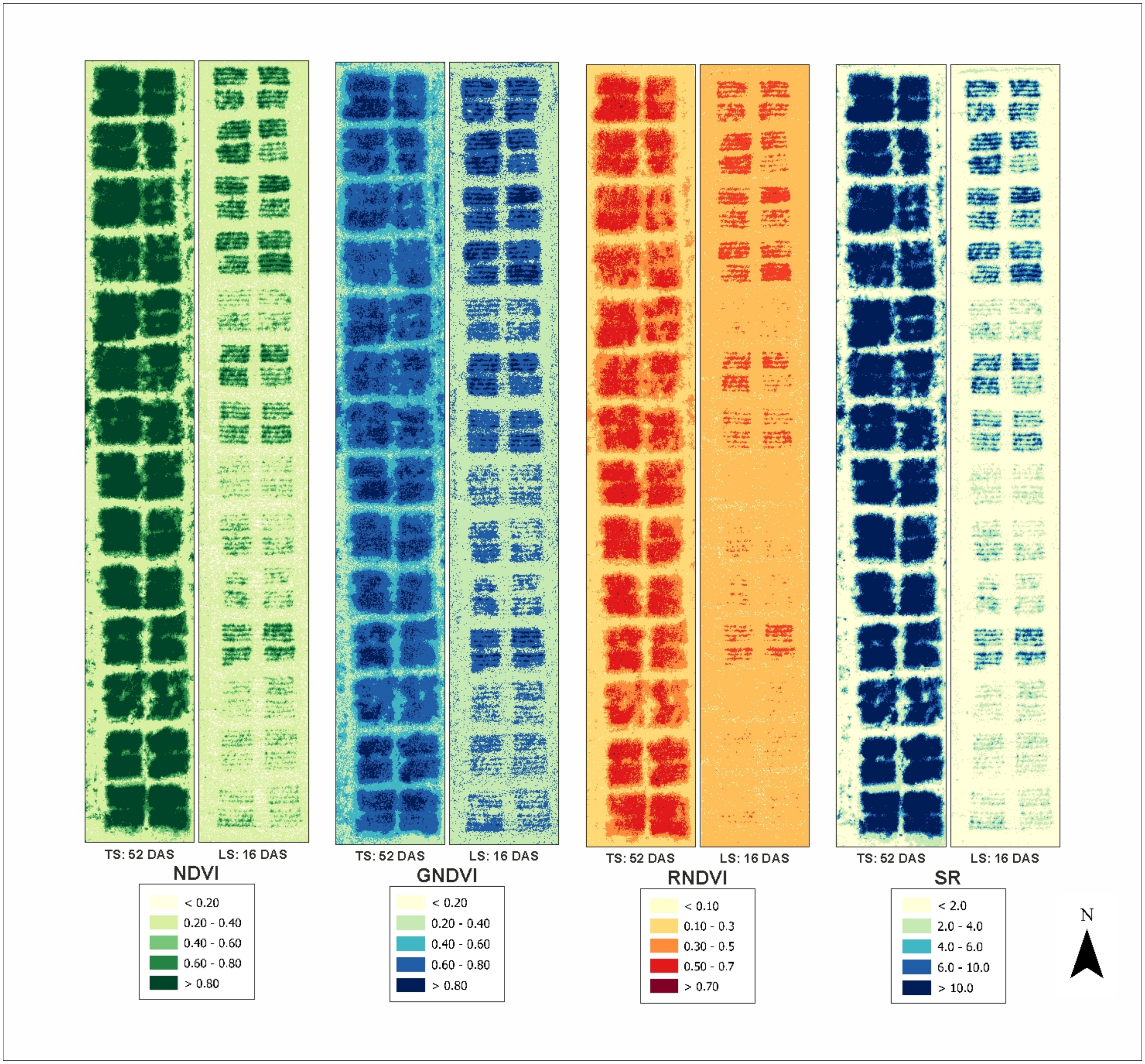

Figure 1

Spatial distribution maps of NDVI, GNDVI, RNDVI, and SR at 52 DAS under TS and 16 DAS under LS conditions

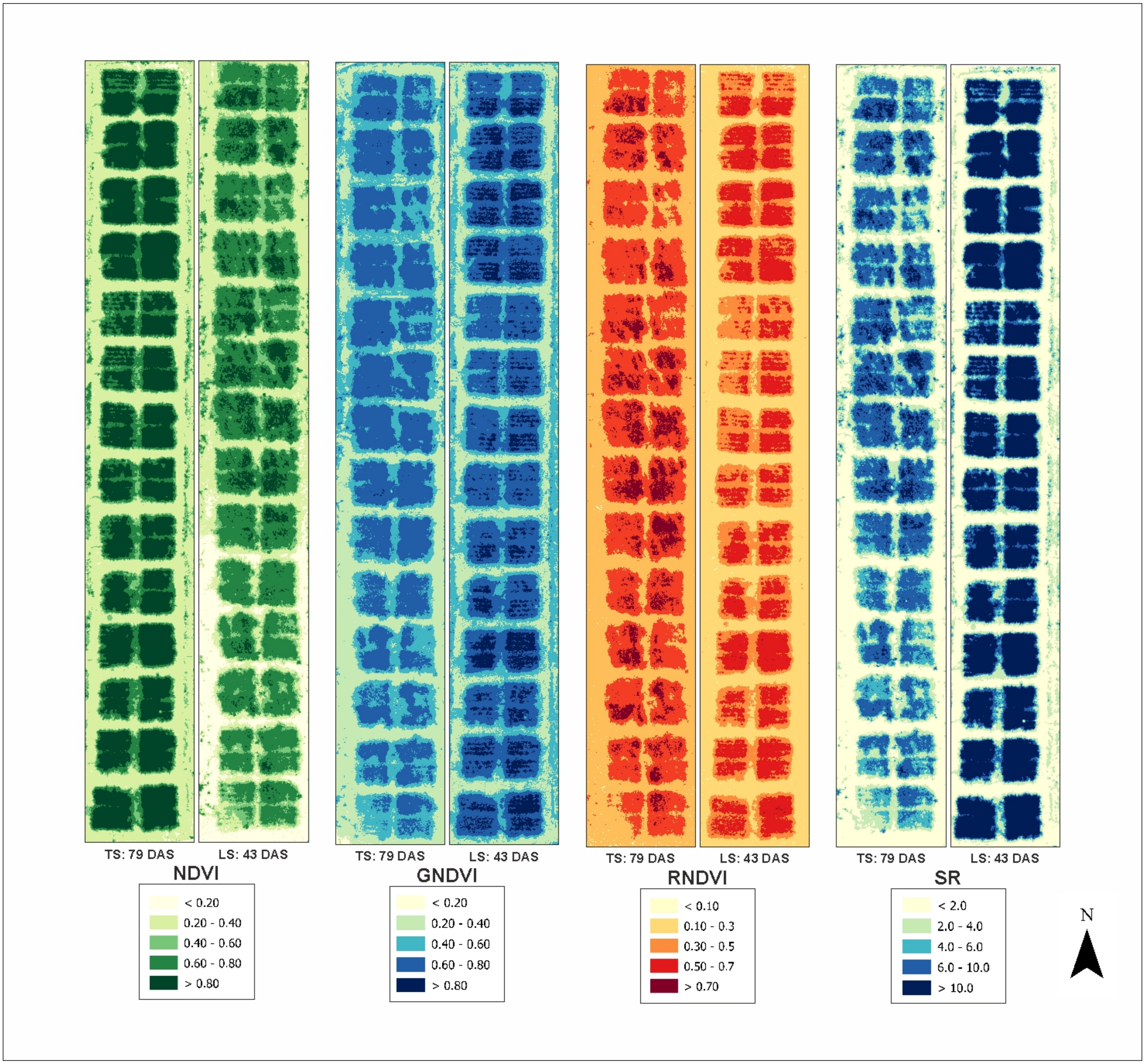

Figure 2

Spatial distribution maps of NDVI, GNDVI, RNDVI, and SR at 79 DAS under TS and 43 DAS under LS conditions

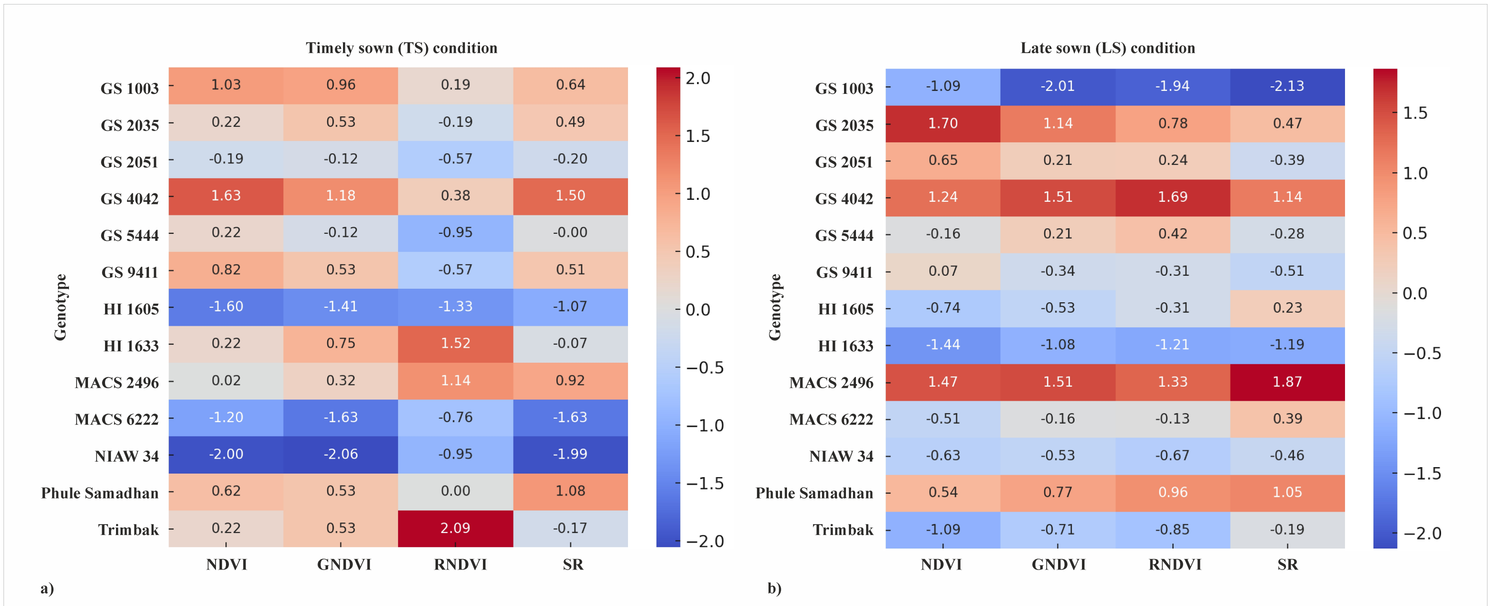

Figure 3

NDVI estimated from aerial multispectral sensor and handheld GreenSeeker crop sensor a) timely sowing; b) late sowing

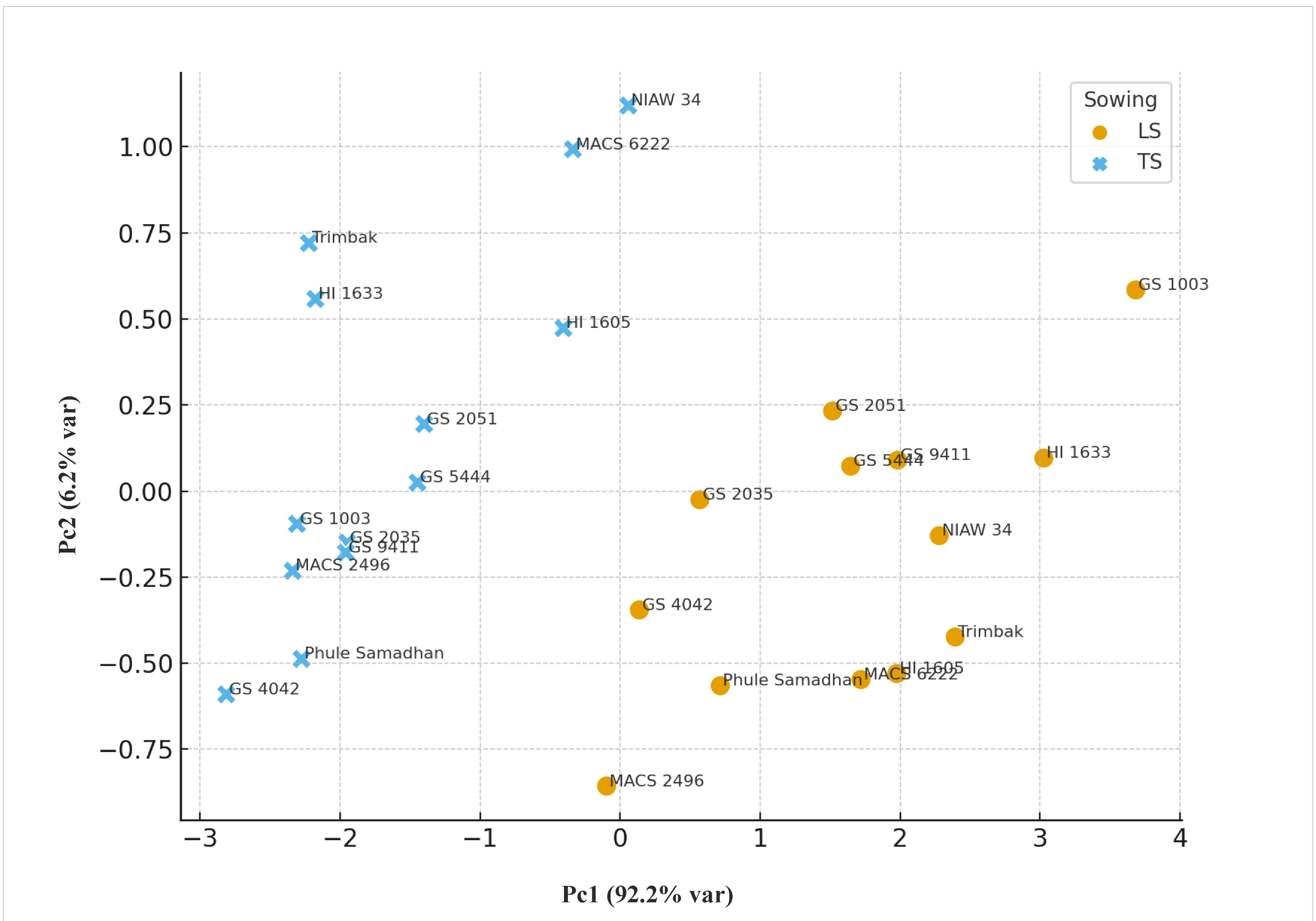

Figure 4

Principal component analysis of vegetation indices under timely and late sowing conditions

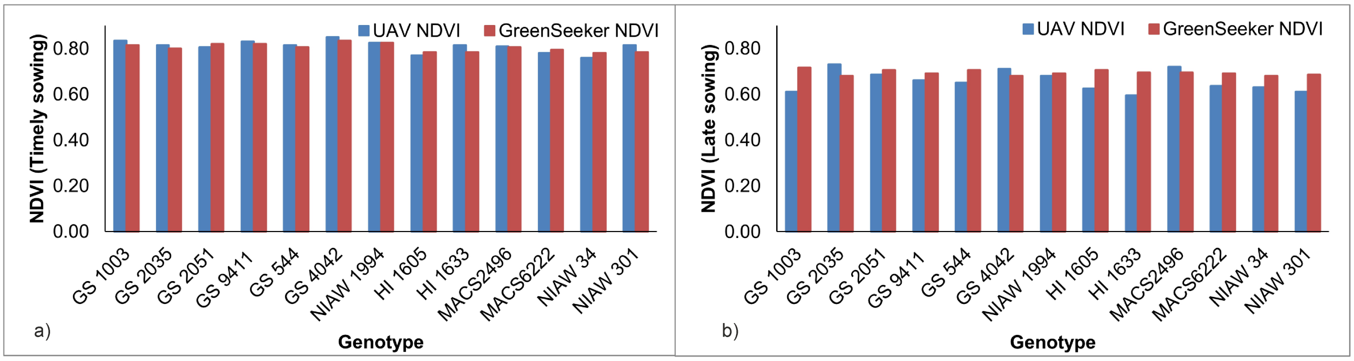

Figure 5

Comparison of UAV-derived and handheld NDVI under timely and late sowing conditions

Supplementary Files

This is a list of supplementary files associated with this preprint. Click to download.

- SupplementaryFigS1.jpg
- SupplementaryFigS2.jpg